[illegible]

Artem Nikonorov, Roman Skidanov, Vladimir Fursov, Maksim Petrov, Sergey Bibikov, Yuriy Yuzifovich

Samara State Aerospace University
34, Moskovskoye Shosse, Samara, Russia, 443086

Image Processing Systems Institute of RAS
151, Molodogvardeyskaya str., Samara, Russia, 443001

artniko@gmail.com romans@smr.ru fursov@ssau.ru max.vit.petrov@gmail.com bibikov.sergei@gmail.com yuriyvyuzifovich@gmail.com

Abstract

This paper describes a unified approach to correct optical distortions in images formed by a Fresnel lens with computational post-processing that opens up new opportunities to use Fresnel lenses in lightweight and inexpensive computer vision devices. Traditional methods of aberration correction do not address artifacts introduced by a Fresnel lens in a systematic way and thus fail to deliver image quality acceptable for general-purpose color imaging. In our approach, the image is restored using three steps: first, by deblurring the base color channel, then by sharpening other two channels, and finally by applying color correction. Deblurring and sharpening remove significant chromatic aberration and are similar to the restoration technique used for images formed by simple refraction lenses. Color correction stage removes strong color shift caused by energy redistribution between diffraction orders of Fresnel lens. This post-capture processing was tested on real images formed by a four-step approximation of the Fresnel lens manufactured in our optics laboratory.

1. Introduction

Modern camera lenses have become very complex. They typically consist of a dozen or more elements to remove optical aberrations [1]. Recently, simple lenses with one or two optical elements were proposed [2]. These lenses are similar to lenses used hundreds years ago, where various aberrations, especially chromatic aberrations, are addressed in post-processing. Recently proposed post-processing techniques can significantly reduce the distortions [2]. With a computational correction, simple lenses can make optical systems inexpensive and lightweight.

Fresnel lenses can be used as imaging lenses and offer a further improvement in weight and linear size to quality ratio over refractive lenses. This advantage is especially pronounced for long focal lengths, where a single Fresnel lens can replace a complex set of refractive lenses. For example, the weight of a typical 300mm lens exceeds 1 kg, while an equivalent Fresnel lens can weigh less than 50 grams. It is also easy to fabricate Fresnel lenses with an aspheric wavefront.

Figure 1: An image formed by a binary Fresnel lens (left); an image formed by a four-step Fresnel lens approximation with computational correction.

However, these advantages come at a cost: the resulting point spread function depends on the light wavelength and has multiple distortions such as moiré and chromatic halo. As a result, Fresnel lenses are typically used as optical collimators or concentrators and not as imaging lens [3]. Other common applications include chromatic aberration compensation using doublets with refractive lenses [4], and as an element in X-Ray microscopes [5, 6].

Fresnel lenses have stronger chromatic aberration than simple refractive lenses do. One of the color channels (in this paper we use the green channel) has less blurring and can be used as a reference channel for the correction of the other two channels. In this paper, we also discuss light energy redistribution between diffraction orders that cause strong chromatic shift.

Chromatic aberrations in distorted images can be algorithmically corrected based on the blind or semi-blind deconvolution [2], or with a sharpening based on contour analysis in different color channels [7]. In [8], a combined technique is used.

Chromatic aberration model is derived as a generalization of optical system defocus model. Richardson [9] and Lucy [10] proposed iteration

deconvolution method for optical defocus compensation in astronomical observations. In recent years, a modified approach is used to correct chromatic aberration [8, 11, 12].

We use both deblur and sharpening to remove chromatic aberrations from images formed with Fresnel lenses. Then we apply color correction based on technique proposed in [13] to remove strong chromatic shift.

Fresnel lens is an approximation of lens surface as shown in Figure 2. We use a four-step approximation of the Fresnel lens created by consecutive etching with different binary masks [14]. Finally, we show the results of the computational correction applied to real images formed by Fresnel lens to prove that this alternative optics can be used in imaging applications. A comparison between image captured by binary Fresnel lens and image captured by our four-step Fresnel lens approximation with computational post-capture processing is shown in Figure 1.

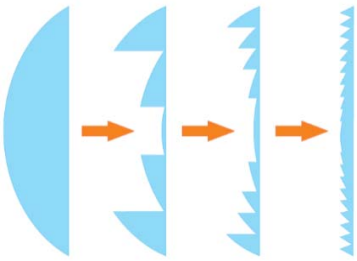

Figure 2: Conceptual illustration of collapsing aspheric refraction lens into Fresnel lens.

2. Image capturing through Fresnel lens

A Fresnel lens used in this work was fabricated using photolithography with spatial resolution of 800nm [15]. Three steps of thermo-chemical thin chrome films writing where used before plasma-chemical etching. An image of the central part of the manufactured Fresnel lens, obtained with white light interferometer (New View Zygo 5000), is shown in Figure 3.

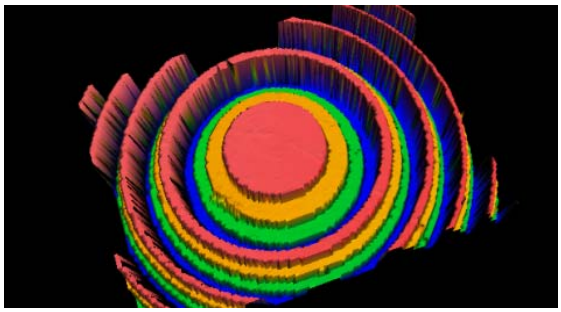

Figure 3: Central part of produced Fresnel lens.

This fabrication technique can produce Fresnel lenses with an aperture of up to *f*/2. Diffraction efficiency of these lenses is close to 80% for the base wavelength.

Chromatic distortions for this lens exceed the distortions produced by refraction lens. Focus distance of the Fresnel lens depends on the wavelength of incident light. Phase zone plate calculated for the base wavelength λ_0, and maintaining focal length f_0 for this wavelength will focus light of wavelength λ on focal distance f, defined by the following expression:

$$f = f_0 \frac{\lambda_0}{\lambda}. \quad (1)$$

A Fresnel lens typically adds strong chromatic distortion in non-monochromatic light. For wavelength further away from λ_0, diffraction efficiency of the zero order decreases. The light focused in the zero order creates an additional chromatic highlight. This highlight becomes stronger as the wavelength deviates from λ_0. Diffraction efficiency of zero order can be expressed as:

$$\tau = \tau_0 \cos^2\left[(n-1)h\frac{\pi}{\lambda}\right], \quad (2)$$

where τ is transmittance coefficient in the zero order direction, τ_0 total lens transmittance coefficient, h - height of Fresnel lens microrelief, n – refraction index. We will call the color highlights caused by the energy focused in non-working diffraction orders as *chromatic shift*, in addition to chromatic aberration. Chromatic aberration leads to color fringe along the edges and color shift distort colors of plane colored parts of the image.

We use first diffraction order as work order. We made numerical simulations of focusing process of binary Fresnel lens. As shown in Figure 4, focusing distance shifts for wavelengths deviated off the base wavelength. This shift leads to axial chromatic aberration. When a certain wavelength is out of focus, the energy passes to different diffraction orders, causing additional chromatic shift.

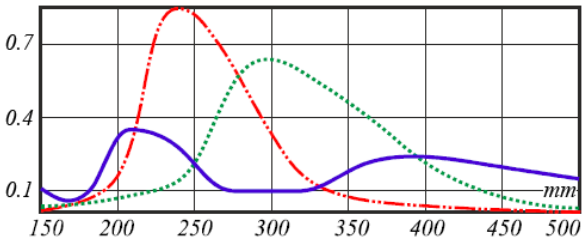

Figure 4: Intensity distribution on the optical axis of binary Fresnel lens (blue line for λ=400 nm, green – for 550 nm and red for 700 nm).

In the next section, we introduce a distortion model as the foundation for the step-by-step computational correction of chromatic aberrations and chromatic shift.

3. Image correction for Fresnel lenses

Chromatic aberration in refraction lenses is described by the general defocus model [2]. In this model, the blur kernel, or point spread function (PSF), is supposed to be linear, at least in local spatial area, as shown in:

$$p^{B}_{RGB}(\mathbf{x}) = \mathbf{B} \otimes p^{0}_{RGB}(\mathbf{x}) + \mathrm{n}\,, \quad (3)$$

where $p^{B}_{RGB}(\mathbf{x})$ is the one of the red, green, or blue color channels of the blurred image, and $p^{0}_{RGB}(\mathbf{x})$ is the corresponding color channel of the underlying sharp image, $\mathbf{B}$ is a blur kernel, or PSF, n is additive image noise, $\mathbf{x} \in \mathbf{Z}^2_+$ is a point in image spatial domain.

Paper [16] shows that the lens PSF varies substantially being a function of aperture, focal length, focusing distance, and illuminant spectrum. So, the assumption that the blur kernel B in (3) is constant is not accurate enough, especially for Fresnel lenses with strong chromatic aberration.

For a strong aberration, kernel B is space-varying. There are two types of distortions in the image: space-varying chromatic blur along the edges and color shift in the regions with plain colors. Therefore, we use the following modification of (3) to handle these distortions:

$$p^{D,B}_{RGB}(\mathbf{x}) = \mathbf{B}_{RGB} \otimes p^{D}_{RGB}(\mathbf{x}) + \mathrm{n}, \quad (4)$$

$$p^{D}_{RGB}(\mathbf{x}) = D_{RGB}(p^{0}_{RGB}(\mathbf{x})). \quad (5)$$

Here $p^{D,B}_{RGB}(\mathbf{x})$ are color channels of the image captured through Fresnel lens; $D_{RGB}(p^{0}_{RGB}(\mathbf{x}))$ is a component characterizing the color shift, caused by energy redistribution between diffraction orders. Blurring kernels $\mathbf{B}_{RGB}$ in (4) are different for different color channels; let us call these kernels the chromatic blur.

An example of effect of chromatic aberrations and chromatic shift for the captured image and its channels is shown in Figure 5, and Figure 11. Schematic model of distortions caused by Fresnel lens is shown in Figure 6.

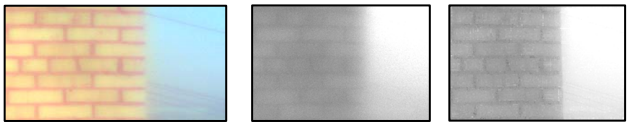

Figure 5: Example of chromatic distortions – distorted RGB image, its blue channel before and after correction.

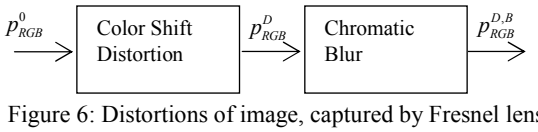

Figure 6: Distortions of image, captured by Fresnel lens.

According to (4), the correction consists of two stages – removing the chromatic blur and the correction of the color shift. To correct chromatic blur, we will use both deconvolution and sharpening. At first, we obtain deblurred green channel, the sharpest one, by a deconvolution:

$$p^{D}_{G}(\mathbf{x}) = \mathbf{B}^{-1}_{G} \otimes \left(p^{D,B}_{G}(\mathbf{x}) \right). \quad (6)$$

Here operation $\mathbf{B}^{-1}_{k} \otimes$ is a deconvolution for the chromatic deblurring, with an intermediate image $\mathbf{p}^{D}_{G}(\mathbf{x})$ as a result.

Then we apply a sharpening to red and blue channels using deblurred green channel as a base:

$$p^{D}_{RB}(\mathbf{x}) = S(p^{D,B}_{RB}(\mathbf{x}), p^{D}_{G}(\mathbf{x}))\,. \quad (7)$$

Finally, we apply color correction to the obtained image:

$$p_{RGB}(\mathbf{x}) = F(p^{D}_{RB}(\mathbf{x}), p^{D}_{G}(\mathbf{x}))\,. \quad (8)$$

$F(p^{D}_{RB}(\mathbf{x}), p^{D}_{G}(\mathbf{x}))$ is a color correction transformation. Similar to sharpening, we use information available in the green channel to correct color shift in red and blue channels.

Combining the above steps, we propose the following technique based on model (4) - (5):

1) the chromatic deblurring (6) of the green channel based on the deconvolution, described in Section III);

2) the chromatic sharpening (7) of the blue and red channels using the contours analysis (this approach is described in Section IV);

3) the color correction (8) to remove color shift, which is described in Section V.

These three steps of post-capturing correction are shown in Figure 7.

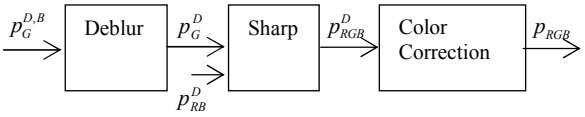

Figure 7: Post-captured computational correction.

4. Primal-dual deconvolution algorithm for chromatic deblurring

To solve the image deconvolution problem (7), we base our optimization method on the optimal first-order primal-dual framework by Chambolle and Pock [17], whose original paper we recommend for an in-depth description. In this section, we present a short overview of this optimization.

Let U and V be finite-dimensional real vector spaces for the primal and dual space, respectively. Let's consider the following operators and functions:

$\mathbf{K} : \mathrm{U} \to \mathrm{V}$ is a linear operator from U to V;

$\mathbf{G} : \mathrm{U} \to [0, +\infty)$ is a proper, convex, lower-semicontinuous (l.s.c.) function [17];

$\mathbf{F} : \mathrm{V} \to [0, +\infty)$ is a proper, convex, (l.s.c.) function.

The optimization framework of (5) considers general problems of the form

$$\hat{\mathbf{u}} = \arg\min_{\mathbf{u}} \mathbf{F}(\mathbf{K}(\mathbf{u})) + \mathbf{G}(\mathbf{u}). \quad (9)$$

To solve the problem in the form (9), the following algorithm is proposed in paper [17].

Initialization step: choose $\tau, \sigma \in R_+$, $\theta \in [0,1]$, $(\mathbf{u}_0, \mathbf{v}_0) \in \mathrm{U} \times \mathrm{V}$ – some initial approximation, $\bar{\mathbf{u}}_0 = \mathbf{u}_0$.

Iteration step: $n \geq 0$, iteratively update $\mathbf{u}_n, \mathbf{v}_n, \bar{\mathbf{u}}_n$ as follows:

$$\mathbf{v}_{n+1} = prox_{\sigma F^*}(\mathbf{v}_n + \sigma \mathbf{K}\bar{\mathbf{u}}_n), \quad (10)$$

$$\mathbf{u}_{n+1} = prox_{\tau \mathbf{G}}(\mathbf{u}_n + \tau \mathbf{K}^* \mathbf{v}_{n+1}), \quad (11)$$

$$\bar{\mathbf{u}}_{n+1} = \mathbf{u}_{n+1} + \theta(\mathbf{u}_{n+1} - \mathbf{u}_n). \quad (12)$$

Following paper [17], a proximal operator with respect to **G** in (11), is defined as:

$$prox_{\tau \mathbf{G}}(\hat{\mathbf{u}}) = (\mathbf{E} + \tau \partial \mathbf{G})^{-1}(\hat{\mathbf{u}}) = \\ = \arg\min_{\mathbf{x}} \frac{1}{2\tau} \|\mathbf{u} - \hat{\mathbf{u}}\|_2^2 + \mathbf{G}(\mathbf{u}), \quad (13)$$

where **E** is identity matrix. The proximal operator in (10) $prox_{\sigma F^*}$ is defined in a similar way.

In order to apply the described algorithm to the deconvolution of the green channel (6), we follow [17]:

$$\mathbf{F}(\nabla p_G^{D,B}) = \left\| \nabla p_G^{D,B} \right\|_1, \quad (14)$$

$$\mathbf{G}(p_G^D) = \left\| \mathbf{B}_G \otimes p_G^D - p_G^{D,\mathrm{B}} \right\|_2^2. \quad (15)$$

Using (14) and (15), it is possible to obtain the proximal operators for steps (10) and (11) of the algorithm. Further details are available in [17]. The deconvolution algorithm based on the total variance can preserve sharp edges.

This deconvolution step is applied to the green channel as shown in (6). The other two channels are restored using sharpening procedure (7) described in the next section.

5. Chromatic sharpening using color contour processing

We propose a modification of the algorithm [7] to sharpen red and blue channels based on the deblurred green channel. This algorithm makes transition areas along the edges in red and blue channels look similar to transition areas in the green channel. An example of this area is shown in Figure 8. For this algorithm to work properly, edges must be achromatic [22]. While this is not always the case, we must rely on this assumption because we need to get strong chromatic blur removed in red and blue channels (shown in Figure 11(f)).

The original algorithm is based on the contour analysis. One of the color channels is used as a reference channel, a green channel in our case. Here we will consider one row of the image pixels with fixed x_2. Below in this section we will use one-dimensional indexing for clarity.

We will search for the edges in the green channel. Let x_c be the first detected transition point in the green channel, such as $|\nabla p_G(x_c)| \geq T$, where T – a certain threshold value. Let us consider a certain neighborhood of $x_c - N$:

$$B(x) = \max_{x \in N} sign(\nabla p_G(x_c)) \nabla p_{RGB}(x). \quad (16)$$

Required transition zone $N_C(x_c)$ is defined as follows:

$$N_C(x_c) = \{x : B(x) \geq \mathrm{T}, x \neq x_c\}. \quad (17)$$

Let l_C be the left border, and r_C be the right border of this area.

In the transition area, an abrupt change of values in red or blue or both color channels occurs. The algorithm transforms signals in red and blue channels to match the signal in the green channel in the transition area $N_C(x_c)$ as closely as possible.

To do this, we define differences between signals:

$$d_{RB}(x) = p_{RB}(x) - p_G(x). \quad (18)$$

For each pixel $x \in N_C$, these differences must be smaller than the differences on the border of the transition area. If this is not the case, red and blue components of these pixels need to be corrected in one of the following ways.

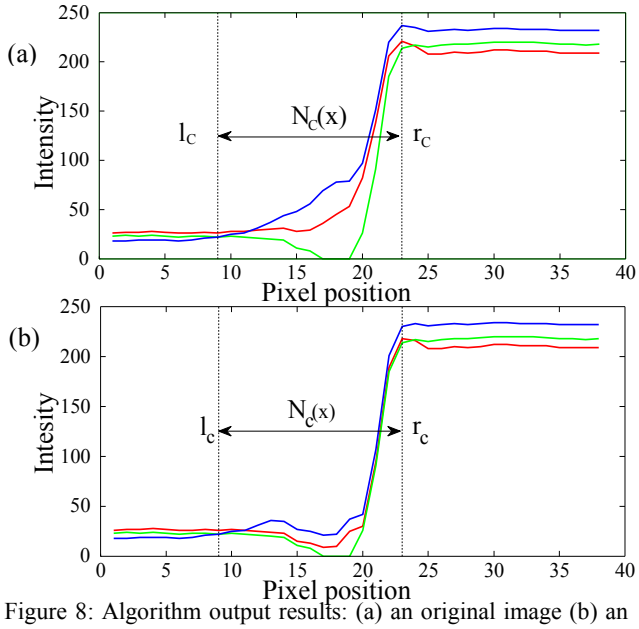

Figure 8: Algorithm output results: (a) an original image (b) an image after color contour processing.

If the color difference between channels (18) at a pixel $x \in N_C$ is higher than the maximum of color difference on the borders

$$d_{RB}(x) \geq \max(d_{RB}(l_C), d_{RB}(r_C)), \quad (19)$$

then

$$S_{RB}(x) = \max(d_{RB}(l_C), d_{RB}(r_C)) + p_G(x). \quad (20)$$

Else, if $d_{RB}(x)$ is smaller than the minimum of color difference on the borders

$$d_{RB}(x) \le \min\left(d_{RB}(l_C), d_{RB}(r_C)\right), \quad (21)$$

then

$$S_{RB}(x) = \min\left(d_{RB}(l_C), d_{RB}(r_C)\right) + p_G(x). \quad (22)$$

We don't use sharpening for intermediate values, if

$$\max\left(d_{RB}(l_C), d_{RB}(r_C)\right) > d_{RB}(x), \quad d_{RB}(x) > \min\left(d_{RB}(l_C), d_{RB}(r_C)\right), \quad (23)$$

then

$$S_{RB}(x) = 0. \quad (24)$$

Therefore, color differences d_{RB} decrease, and red and blue signals in the transition area look more similar to G. An example of algorithm output is shown in Figure 8(b).

There are several pixels with close to zero values in the green channel, pixels #16-19 in Figure 8(a). This means that there is no significant information in the green channel for pixel correction in red and blue channels in this part of the transition area. We propose the following algorithm to solve this problem:

1) We use a median filter to preprocess the green channel in order to handle close to zero values. We replace a pixel with a close to zero value to the middle value in a neighboring window. If the new value is also close to zero, the window size of the median filter increases.

2) We compute the matrix of the correction coefficients $R_{RB}(\mathbf{x})$ for the whole image. Then we apply the post processing steps 3) and 4) to the $R_{RB}(\mathbf{x})$ values.

3) Applying grayscale dilation [21] to matrices of sharpening values $S_{RB}(\mathbf{x})$.

4) Limiting excessively bright pixels to values allowed inside the transition area.

Finally we sharpen red and green channels using the following rule:

$$p_{RB}^{D}(\mathbf{x}) = \begin{cases} S_{RB}(\mathbf{x}), & S_{RB}(\mathbf{x}) \neq 0; \\ p_{RB}^{D,B}(\mathbf{x}), & S_{RB}(\mathbf{x}) = 0. \end{cases} \quad (25)$$

After deblurring green channel and sharpening red and blue channels, we use color correction, described in the following section, to remove the strong color shift caused by the energy redistribution between diffraction orders.

6. Color correction of chromatic shift

At the end of the image restoration sequence, we apply color correction (8). Here we apply single-channel correction described in [13], only modified to use green channel information as an additional input for red and blue channel transformations. As shown in [13], the problem consists of correcting non-isoplanatic deviation in illumination $I(\lambda, \mathbf{x})$ and restoring an image with the given illumination $I_0(\lambda)$:

$$\mathbf{p}(\mathbf{x}) = \int R(\lambda, \mathbf{x}) I(\lambda, \mathbf{x}) \mathbf{T}(\lambda, \mathbf{x}) d\lambda \rightarrow \rightarrow \mathbf{p}_0(\mathbf{x}) = \int R(\lambda, \mathbf{x}) I_0(\lambda) \mathbf{T}(\lambda) d\lambda, \quad (26)$$

where R and I are $R \times \mathbf{Z}_2 \rightarrow [0,1]$ functions of wavelength λ. R is the spectral reflectance of the scene surfaces. **I** is the spectral irradiance that is incident at each scene point. $\mathbf{T}(\lambda) = [T_R(\lambda), T_G(\lambda), T_B(\lambda)]^T$ is the spectral transmittance distribution of color sensors. In [13] it was shown that task (26) could be solved by finding the correction function *F()*.

We propose using prior knowledge of the colors of small isolated patches in the image in the same way as any color correction specialist would do. These small neighborhoods, limited in color and space, are defined in [13] as spectral shape elements, or in trichromatic, RGB, case, as color shape elements, CSE. This model was useful for both color correction and artifacts removing problems [18].

Using CSE, the task of the color correction function identification takes the following form:

$$\mathbf{a}^* = \arg\min_{\mathbf{a}} \left\| F(\mathbf{u}_i, \mathbf{a}), \mathbf{u}_i^0 \right\|, \quad (27)$$

where $\{\mathbf{u}_i\}$ is a set of distorted SSE, and $\{\mathbf{u}_i^0\}$ is a set of distortion-free CSE. Hausdorff-like measure between CSEs in three dimensional color space is used as a metric $\| \ , \ \|$ in (27). General form for this metric is:

$$\left\| \mathbf{u}_i, \mathbf{u}_j \right\| = \max \begin{pmatrix} \max\limits_{\mathbf{x} \in \mathbf{u}_i} \min\limits_{\mathbf{y} \in \mathbf{u}_j} \left| \mathbf{p}(\mathrm{x}), \mathbf{p}(\mathrm{y}) \right|, \\ \max\limits_{\mathbf{y} \in \mathbf{u}_j} \min\limits_{\mathbf{x} \in \mathbf{u}_i} \left| \mathbf{p}(\mathrm{x}), \mathbf{p}(\mathrm{y}) \right| \end{pmatrix}, \quad (28)$$

where $|,|$ is a distance in color space. We use separate parameter estimation (27) for each color channel.

Since we use a channel-wise correction procedure, metric (28) can be calculated using only two values for each color channel independently, and (27) takes a following form for each color channel p:

$$\mathbf{a}^* = \arg\min_{\mathbf{a}} \left\| F(p_k, \mathbf{a}), p_k^0 \right\|, \quad (29)$$

$$\mathrm{p}_k = \min p(\mathbf{u}_i), \ \mathrm{p}_{k+1} = \max p(\mathbf{u}_i), \quad (30)$$

$$\mathrm{p}_k^0 = \min p(\mathbf{u}_i^0), \ \mathrm{p}_{k+1} = \max p(\mathbf{u}_i^0). \quad (31)$$

Assuming that the distortions are described by a bi-illuminant dichromatic model [19] of the following form:

$$\mathbf{p}(\mathbf{x}) = \int H(\mathbf{x}) I(\lambda) R(\lambda, \mathbf{x}) \mathbf{T}(\lambda) d\lambda + \int I(\lambda, \mathbf{x}) R_S(\lambda, \mathbf{x}) \mathbf{T}(\lambda) d\lambda + \int \left(I_A(\lambda) R(\lambda, \mathbf{x}) + \mathrm{S}(\lambda, \mathbf{x}) \right) \mathbf{T}(\lambda) d\lambda, \quad (32)$$

where $I(\lambda) R(\lambda, \mathbf{x})$ is diffuse reflection, $I(\lambda, \mathbf{x}) R_S(\lambda, \mathbf{x})$ a specular reflection, and an ambient light is $I_A(\lambda)$, $H(\mathbf{x})$

is an attenuation factor, and $S(\lambda, \mathbf{x})$ is added to describe color shift caused by energy redistribution between diffraction orders.

For the distortions described by this model, the CSE matching condition theorem from [19] can be proven with the following condition applied to the ambient and direct illuminant. If inequality $p_k(\mathbf{x}_1) \le p_k(\mathbf{x}_2)$ is true under both illuminants, then it should remain true under ambient illuminant only.

Using the necessary condition from this theorem, the identification problem of the correction function will look as follows:

$$\mathbf{a}^* = \arg\min_{\mathbf{a}}((F(p_k, \mathbf{a}) - p_k^0)^2), \quad F'(p_k, \mathbf{a}) \ge 0. \tag{33}$$

In the problem of color correction for Fresnel lenses, we use a color checker scale, shown in Figures 11(d) and 11(h), for correction identification of each color channel. The original colors of the scale are used as distortion-free CSE, $\mathbf{u}_i^0$. The same scale captured using a Fresnel lens is used for getting distorted CSEs, $\mathbf{u}_i$.

Applying expression (33) we assume that corrected value of each color channel depends only on its distorted value, and it is true for distortions described by dichromatic model (32). However, chromatic shift, caused by the light from different diffraction orders, varies across different color channels.

Histograms in Figure 9(a) present these shifts for the image captured when in focus in green channel. For this example, the green channel is in focus and the blue channel is near focus. The red channel is far from focus, therefore we have a strong red highlight, causing the shift of the red histogram; a similar but smaller shift is present in the blue channel too.

(a)

(b)

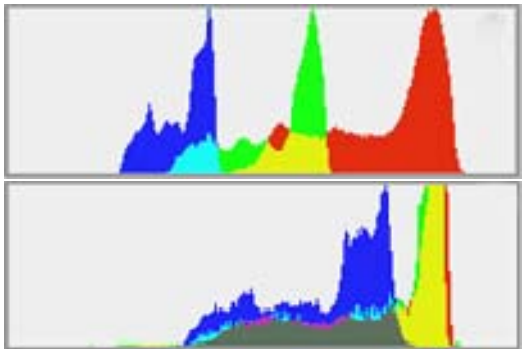

Figure 9: RGB color histograms show different color channel brightness of (a) a Fresnel lens captured image, (b) the same image after correction.

To correct this kind of distortion we use a cross-channel prior. We estimate a parametric dependency between the green channel and each of the other two channels of the following form:

$$\mathbf{b}^* = \arg\min_{\mathbf{b}}(b_1 p_G p_{RB} + b_0 - p_{RB}^0)^2. \tag{34}$$

Note, that we use separate estimation of parameters vector $\mathbf{b}$ for each color channel. Then, each channel is corrected using this estimation of the cross-channel correction transform. This step is applied before estimating the color correction transform (33). Incorporating this cross-channel prior in color is the main distinction from [18].

After performing correction using cross-channel prior (6.9), the problem (33) can be solved for polynomial representation of $F()$. However, the distortions caused by the aberrations in the simple Fresnel lens are too strong. To improve color correction quality, we apply additional conditions.

First, we add two boundary conditions for $F()$: at the starting point it is set to zero, while at the end is set to one:

$$F(0, \mathbf{a}) = 0, \quad F(1, \mathbf{a}) = 1. \tag{35}$$

Because these conditions cannot be applied to a polynomial representation of $F()$, we use cubic smoothed splines with boundary conditions (35)

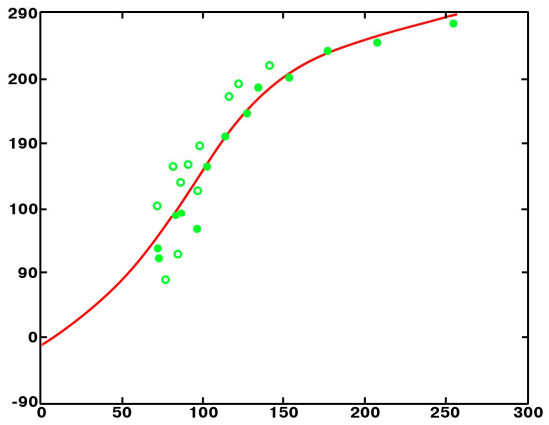

Figure 10: Chromatic shift correction curve for green channel, solid points for inliers CSEs, pitted – for outliers.

Second, as it is shown in Figure 10, initial SSEs set is too noisy, and some data points must be dropped. A classical algorithm for noisy data selection with dropping outliers is RANSAC algorithm. We use a slightly modified RANSAC-based scheme:

1) Select a subset of the initial set.

2) Using this subset, estimate cubic smoothing spline parameters for $F()$ according to (33), (35).

3) For each pair of SSEs, the following inequality can be computed:

$$\left\| F(\mathbf{u}_i, \mathbf{a}), \mathbf{u}_i^0 \right\| \le t \tag{36}$$

where t is a certain threshold. Inequality (36) is true for inlier CSE pairs and false for outliers.

After the color correction transform parameters are identified we apply this transformation to the image as the

final step of the technique based on the model (6) - (8).

To check correction quality we use the following measure:

$$q = \max_i \max_{\mathbf{x}_j \in \mathbf{u}_i} \left\| \mathbf{p}_0(\mathbf{x}_j), \mathbf{p}(\mathbf{x}_j) \right\|_2 \quad (37)$$

where $\|\,,\|_2$ is Euclidian distance between colors of corresponding points of two CSEs – source $\mathbf{p}_0(\mathbf{x}_j)$ and corrected $\mathbf{p}(\mathbf{x}_j)$. We know the matching between the source and the corrected point for color checker tables. This usually unavailable knowledge allows us to estimate the value of the quality measure (37).

7. Results

We applied suggested correction technique to several images and some of the results are shown in Figure 11. The original picture was captured using a digital camera with a single Fresnel lens and sensor resolution of 2048×2048. The lens was made as a four-step approximation of the Fresnel lens. First we removed the blur from the green channel using deconvolution, then we used edge analysis for red and blue channels. We tried pillbox model for the PSF approximation suggested in [8], but decided to use the Gaussian kernel with $\sigma = 2$ because it showed better results with our lens.

Color correction transform applied to the image was identified using a color checker chart (Figures 11(d), 11(h)). The color checker chart and the test image (Figure 11(h)) were captured under similar illumination, close to a standard D50 illuminant.

As it is shown in Figure 11, this correction restores both the color and the edge information in distorted images formed by simple Fresnel lenses. The image captured by a four-step approximation of Fresnel lens is significantly better than the image captured by a binary lens.

Comparison of magnified fragments 10(j), (l) of the test images show that the quality of four-step lens is significantly better than that of the binary lens. While our computational correction improves the quality, certain distortions still remain. Green chromatic deviation is visible over the text, due to less than perfect chromatic deblur. The edge of the color chart patch is somewhat noisy, due to the deconvolution in the green channel.

In Figure 11(c) we include the image taken with a regular refraction lens for reference, clearly showing that there is more work ahead with Fresnel lens, both in manufacturing and post-processing to achieve comparable quality.

We compared our color correction technique with open source implementation of Retinex approach [20]. Results for Retinex-based correction are shown in Figure 11(c). Visual quality of our color correction surpasses the quality of Retinex-based correction. The value of the correction error measure (37) for Retinex is 113 versus 14 for our method.

8. Discussion

Fresnel lens imaging was previously unavailable due to strong chromatic distortions. Only one recent paper [23] uses a binary Fresnel lens for monochrome low-resolution imaging application. We show that a combination of a simple Fresnel lens and a post-processing technique allows us to obtain high-resolution color images comparable to images captured through a refraction lens. We tested a binary, a three- and a four-step approximation of Fresnel lens and only the four-step approximation, after our computational post-processing, allows us to obtain image quality close but not equal to refraction optics, shown in Figure 11(c). An example of the image captured by the binary lens is shown in Figure 11(j) and in Figure 1. The quality of this image is significantly lower than that produced with a four-step Fresnel lens approximation. Binary Fresnel lenses are available from a few manufacturers, such as Edmund Optics, but it can not be used for high-resolution color imaging, due to extreme chromatic aberration. Another kind of a quasi-Fresnel lens is typical plastic engraved lenses, used as magnifying glasses; they are hundreds times thicker than a Fresnel lens. While their chromatic aberration is lower due to thickness, these quasi-Fresnel lenses cannot be used for high-resolution imaging due to other optical aberrations.

Two components of chromatic distortions produced by Fresnel lenses can be corrected by computational post-processing, as described below.

The first distortion component is a longitudinal chromatic aberration, which blurs all color channels except for the green channel. Its correction is based on the debluring of the green channel before sharpening other channels using additional information available in the green channel. Debluring was made by Chambolle and Pock total variance in L_1 metric deconvolution algorithm [17]. This algorithm produces a lower amount of processing noise due to deconvolution.

As it shown in Figure 11 red and blue channels are significantly more blurred than green channel. Our restoration of these channels is based on an assumption that edges are grey [23] and the intensity profiles across the edge are similar for all three color channels. This assumption is widely used in sharpening techniques.

A second distortion component is a strong chromatic shift due to the energy redistribution from different diffraction orders. Correcting for this distortion is based on our color correction technique from [13], and also uses green channel prior to produce correction transform, which is identified with a color checker chart. This chart was captured under the D50 standard illuminant; a real scene was photographed under the same illuminant.

The color checker chart allows us to quantify correction errors. This technique shows a better result,

both by measuring the error and by visual assessment, when compared to a well-known Retinex correction method. However, as shown in Figures 11(a) and 11(c), the quality of the images captured through regular lenses is still superior to our results.

The presented framework of the post-capture processing makes Fresnel imaging possible. As our fabrication technique advances (replacing a three-step lens approximation with a four-step one being one example), the image quality is getting progressively better. However, lens properties change as our production improves, which prevented us from further fine-tuning the post-capturing process.

Due to rapid changes in fabrication, we only use a subset of adaptation techniques in our framework. For example, our color correction was optimized only for the lens sample we had on hands, using calibration under the illuminant in our lab. At the chromatic aberration correction step, only the blur kernel size for the green channel deconvolution was estimated for our lens sample. When our fabrication process stabilizes, we will improve the quality by increasing the accuracy of our deblurring algorithm, taking into account the estimation for the space-varying blur kernel, and by combining sharpening and color correction into a single filter. Another opportunity for quality improvement is to estimate different correction transforms for different illuminations and potentially make our correction illumination-invariant.

9. Acknowledgments

This work was supported by the Ministry of Education and Science of the Russian Federation (grant # 2014/198 and project # RFMEFI57514X0083).

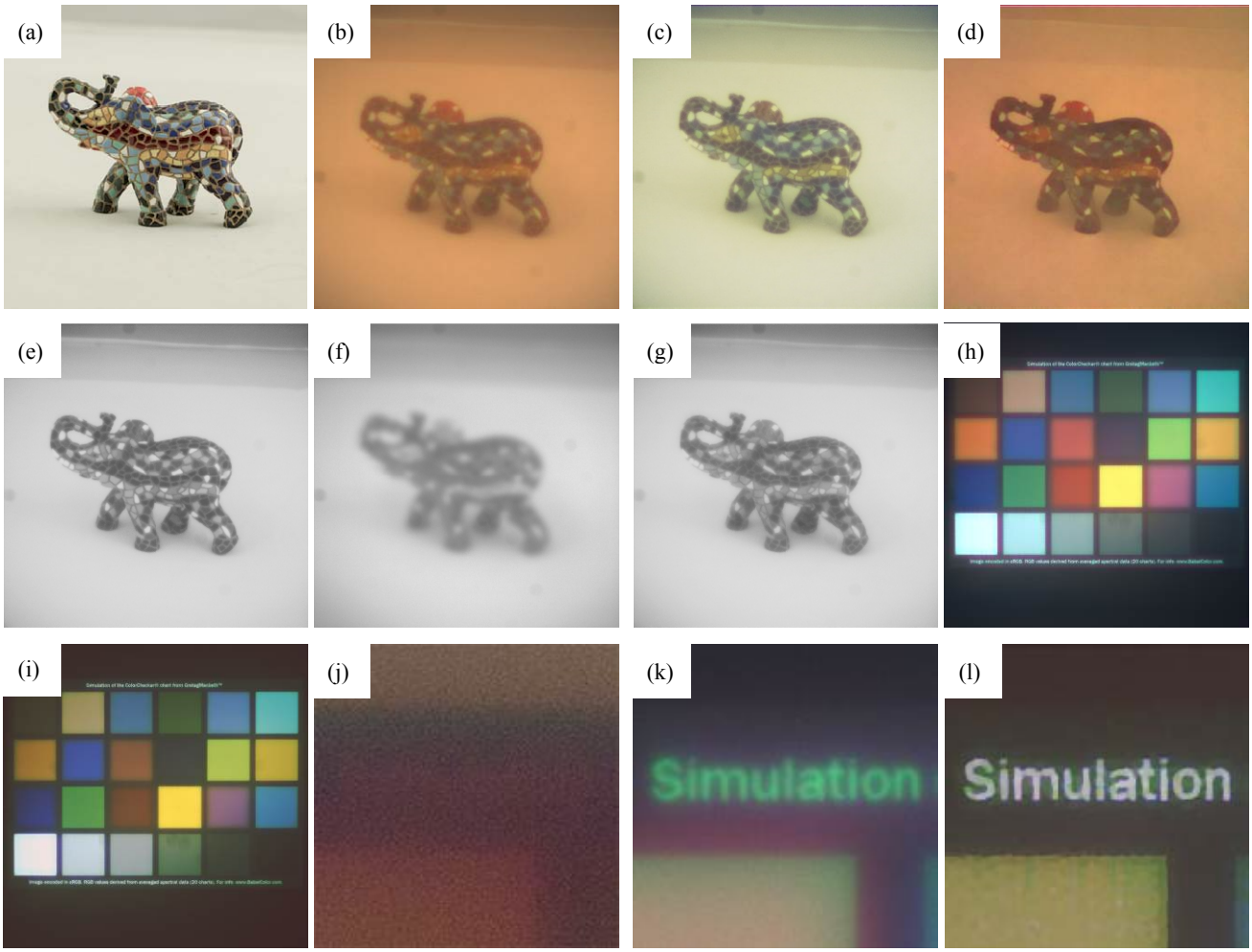

Figure 11: Example of the chromatic aberration correction: (a) – image captured by refraction lens; (b) – image captured by four-step Fresnel lens; (c) – the image after color correction; (d) – the image after a Retinex-based color correction; (e) green and (f) red channels of the captured image; (g) the corrected red channel; (h) - the color chart image for correction identification; (i) – the color chart image after the correction; (j) – part of color chart, captured by binary Fresnel lens; (k) – same part, captured by four-step Fresnel lens; (l) – same part after computational correction.

References

[1] J.R. Meyer-Arendt. Introduction to Classical and Modern Optics, Prentice Hall, 1995.

[2] F. Heide, M. Rouf, M. B. Hullin, B. Labitzke, W. Heidrich, A. Kolb. High-Quality Computational Imaging Through Simple Lenses, ACM Transactions on Graphics 32 (5), No. 149, 2013.

[3] A. Davis, F. Kuhnlenz. Optical Design using Fresnel Lenses – Basic Principles and some Practical Examples, Optik & Photonik 2(4): 52–55, 2007.

[4] G.I. Greisukh, E.G. Ezhov, and S.A. Stepanov. Aberration properties and performance of a new diffractive-gradient-index high-resolution objective, Applied Optics 40(16): 2730-2735, 2001.

[5] J. Thieme. Theoretical Investigations of Imaging Properties of Zone Plates Using Diffraction Theory. X-Ray Microscopy II, Springer Series in Optical Sciences, Volume 56, pages 70-79, 1988.

[6] A. Takeuchi, K. Uesugi, Y. Suzuki, S. Tamura, N. Kamijo. High-Resolution X-Ray Imaging Microtomography with Fresnel Zone Plate Optics at SPring-8, Proc. 8th Int. Conf. X-ray Microscopy IPAP Conf. Series 7: 360-362, 2006.

[7] S.-W. Chung, B.-K. Kim, W.-J. Song. Removing chromatic aberration by digital image processing, Optical Engineering 49(6), 067002, 2010.

[8] S.B. Kang. Automatic Removal of Chromatic Aberration from a Single Image, CVPR 2007, p.1-8, 2007.

[9] W. H. Richardson, Bayesian-based iterative method of image restoration, J. Opt. Soc. Am, 62: 55-59, 1972.

[10] L. Lucy. An iterative technique for the rectification of observed distributions, The Astronomical Journal 79: 745, 1974.

[11] T.S. Cho, N. Joshi, C.L. Zitnick, K.S. Bing, R. Szeliski, W.T. Freeman. A content-aware image prior, IEEE Conference on Computer Vision and Pattern Recognition, p. 169-176, 2010.

[12] T.S. Cho, N. Joshi, C.L. Zitnick, K.S. Bing, R. Szeliski, W.T. Freeman. Image restoration by matching gradient distributions, Pattern Analysis and Machine Intelligence, IEEE Transactions on Pattern Analysis and Machine Intelligence 34(4): 683-694, 2012.

[13] A. Nikonorov, S. Bibikov, P.Yakimov, V. Fursov, Spectrum shape elements model to correct color and hyperspectral images, 8th IEEE IAPR Workshop on Pattern Recognition in Remote Sensing, p. 1-4, 2014.

[14] V.A. Soifer (ed.). Computer Design of Diffractive Optics. Woodhead Publishing. 2012.

[15] L. Kazanskiy, S.N. Khonina, R.V. Skidanov, A.A. Morozov, S.I. Kharitonov, S.G. Volotovskiy Formation of images using multilevel diffractive lens, Computer Optics 38 (3): 425-434, 2014

[16] Y. Shih, B. Guenter, N. Joshi. Image Enhancement Using Calibrated Lens Simulations. ECCV 2012, Lecture Notes in Computer Science 7575: 42-56, 2012.

[17] A. Chambolle, T. Pock A first-order primal-dual algorithm for convex problems with applications to imaging, Journal of Mathematical Imaging and Vision, 40: 120–145, 2011.

[18] A. Nikonorov, S. Bibikov, V. Fursov Desktop supercomputing technology for shadow correction of color images, Proceedings of the 2010 International Conference on Signal Processing and Multimedia Applications (SIGMAP), p. 124-140, 2010.

[19] B.A. Maxwell, R.M. Friedhoff, C.A. Smith. A Bi-Illuminant Dichromatic Reflection Model for Understanding Images, In Computer Vision and Pattern Recognition, IEEE Conference on, p. 1–8, 2008.

[20] N. Limare, A.B. Petro, C. Sbert, J.M. Morel. Retinex Poisson Equation: a Model for Color Perception, Image Processing On Line, 2011.

[21] R.C. Gonzalez, R.E. Woods. Digital Image Processing, Second Edition, Prentice Hall, 2001.

[22] Van de Weijer, J., Gevers, T., Color constancy based on the Grey-edge hypothesis, IEEE International Conference on Image Processing, V.II - pp. 722-725, 2005.

[23] S. K. Nayar, D. C. Sims, M. Fridberg, Towards Self-Powered Cameras, Proceeding of the International Conference on Computational Photography (ICCP), pp.1-10, Apr, 2015.